Co-funded by the European Union

Research Fund for Coal & Steel

Hybrid energy storage system using post-mining infrastructure (HESS)

Deliverable 4.1.

Thermodynamic analysis of the proposed systems

18.12.2024

PROJECT	
Project number	**101112380**
Project name	**Hybrid energy storage system using post-mining infrastructure**
Project acronym:	**HESS**
Call	**RFCS-2022**
Topic	**RFCS-01-2022-RPJ**
Type of action	**RFCS-PJG**
Service	**REA/B/01**

DOCUMENT PROPERTIES

Document Number	D.4.1.
Document Title	**Thermodynamic analysis of the proposed systems**
Document responsible	**SUT**
Target dissemination level	**PU**
Document authors	**Krzysztof Rusin (SUT)** **Jakub Ochmann (SUT)** **Sebastian Rulik (SUT)** **Michał Jurczyk (SUT)** **Łukasz Bartela (SUT)**
Data of the document	**18.12.2024**

Co-funded by the European Union

Research Fund for Coal & Steel

Table of contents

Co-funded by the European Union

Research Fund for Coal & Steel

1. Intruduction

Transformations of the fundamental characteristics of the Polish electricity system result in a reduction in its flexibility and an increased probability of energy supply capacity being lost to the end user. One proposed solution is the implementation of energy storage facilities, which may enhance energy system security [1]. The ongoing decarbonisation process in Central European countries, which also results in the phasing out of mines, offers opportunities to utilise post-mining infrastructure as components of energy storage systems. Potential pathways for the utilisation of post-mining infrastructure as energy storage include the realisation of a compressed air energy storage system (CAES) [2,3] and a compressed carbon dioxide energy storage system (CCES) [4,5].

At present, two commercial CAES systems are in operation worldwide. The first is located in Huntorf, Germany, and the second is situated in Mcintosh, USA. Both utilise salt caverns as compressed air reservoirs. The Huntorf power plant, constructed in 1978, underwent the upgrade in 2007 that increased its capacity from 290 to 320 MW with the efficiency of 42%. The plant was originally designed as a power reserve for a nearby nuclear power plant in the case of power loss. The 110 MW McIntosh power station was commissioned in 1991. Energy storage plants utilise the combustion of natural gas during the discharge stage to increase the enthalpy of the gas before it expands [6]. Figure 1 illustrates a schematic diagram of a CAES-type system employing an underground salt cavern as a compressed air reservoir. Figure 2 presents the Huntorf Power Plant with the highlighted key elements of the system.

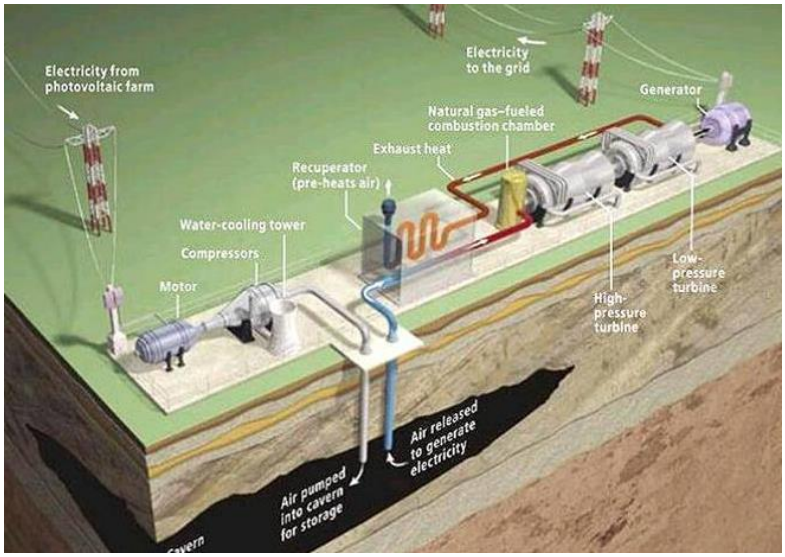

Fig. 1 Visualisation of the compressed air energy storage system [7]

Co-funded by the European Union
Research Fund for Coal & Steel

Fig. 2 Huntorf Power Plant [8]

The experience of energy storage in compressed carbon dioxide is currently limited to conceptual considerations and pilot installations. The primary challenge in implementing these systems is the necessity to construct a sealed installation comprising low and high-pressure vessels that expand and compress the carbon dioxide. The authors of the EnergyDome pilot plant, with a capacity of 2.5 MW and 4 MWh, have reported an efficiency of 75% for their system.

2. Goal of the work

The objective of the present study is to create analytical models of a compressed air energy storage system and a compressed carbon dioxide energy storage system to explore the potential of these systems using mine infrastructure. A comparative analysis will be carried out in order to identify the preferred configurations of the systems in terms of their integration with the energy router.

3. Methodology

3.1. Governing equations

The isentropic efficiency of an air compressor η_{iC} is defined as [3]:

$$\eta_{\mathrm{iC}} = \frac{h_{\mathrm{out\_s}} - h_{\mathrm{in}}}{h_{\mathrm{out}} - h_{\mathrm{in}}}$$

where h_{in} is the enthalpy of the inlet gas to the compressor, and h_{out} and $h_{\text{out\_s}}$ are the enthalpy of the discharge gas from the compressor and the enthalpy of the discharge gas from the compressor, respectively, assuming isentropic gas compression. At the calculation stage, it was assumed that there were relationships between the compressor efficiency and the compression ratio and mass flow of the compressed gas. These relationships were assumed on the basis of literature data [9]. The compressor power N_{C} is defined as:

$$N_{\text{C}} = \frac{N_{\text{i C}}}{\eta_{\text{em\_C}}}$$

where $\eta_{\text{em\_AirC}}$ is the electromechanical efficiency of the compressor unit and $N_{\text{i\_AirC}}$ is the internal power of the compressor defined as:

$$N_{\text{i\_C}} = \dot{m}(h_{out} - h_{in})$$

where $\dot{m}$ is the gas mass flow. The isentropic efficiency of an gas expander η_{iEx} was defined as:

$$\eta_{\text{iEx}} = \frac{h_{\text{in}} - h_{\text{out}}}{h_{\text{in}} - h_{\text{out\_s}}}$$

where h_{in} is the enthalpy of the inlet gas entering the expander, and h_{out} and $h_{\text{out\_s}}$ are the enthalpy of the expander outlet gas and the enthalpy of the expander exhaust gas, respectively, assuming isentropic gas expansion. At the calculation stage, like in the case of the compressor, relationships between the efficiency, the expansion ratio and mass flow rate were assumed. These relationships were assumed on the basis of literature data [9]. The expander power N_{Ex} was defined as:

$$N_{\text{Ex}} = \eta_{\text{em\_Ex}} \cdot N_{\text{i\_Ex}}$$

where $\eta_{\text{em\_Ex}}$ is the electromechanical efficiency of the expander unit and $N_{\text{i\_Ex}}$ is the internal power of the expander defined as:

$$N_{\text{i\_Ex}} = \dot{m}(h_{in} - h_{out})$$

The TES tank was modelled as an element with variable operating parameters during the charging and discharging stages. The performance characteristics of the TES, which have been demonstrated experimentally and numerically [10], indicate that it is impossible to ensure constant air operating parameters when using a porous bed as a heat accumulator. The Ergun equation was used to estimate the value of the pressure drop of air flowing through the TES during the charging and discharging stages [11]:

$$\frac{|\Delta p|}{L} = \frac{150 \cdot \mu}{d_p^2} \cdot \frac{(1-\varepsilon)^2}{\varepsilon^3} \cdot v_\infty + \frac{1.75 \cdot \rho}{d_p} \cdot \frac{(1-\varepsilon)}{\varepsilon^3} \cdot v_\infty^2$$

where L is the length of the TES tank, d_p is the diameter of the porous bed elements, ε is the porosity of the rock bed, v_∞ is the air velocity through the TES tank, ρ and μ are the density and viscosity of the air, respectively. These parameters are dependent on the average air temperature in the TES, which is estimated based on the author's methodology [10].

The round-trip energy efficiency η_{ES} of an energy storage system is calculated from the relationship:

$$\eta_{\mathrm{ES}} = \frac{E_{\mathrm{Ex}}}{E_{\mathrm{C}}}$$

where E_{AirEx} is the electricity production during the discharge stage defined as

$$E_{\mathrm{Ex}} = \int_{\tau_c}^{\tau_d} (N_{\mathrm{Ex}})\, d\tau$$

and E_{AirC} is the electricity consumption during the charging stage defined as:

$$E_{\mathrm{C}} = \int_{\tau_a}^{\tau_b} (N_{\mathrm{C}})\, d\tau$$

In the modelling of the compressed carbon dioxide energy storage system, an index was employed to ascertain the pressure change in the low-pressure CO_2 reservoir, which was defined as follows:

$$\xi_{LPT} = \frac{p_{max} - p_{min}}{p_{min}}$$

3.2. A-CAES configurations tested

- CASE A

System description: During the charging stage, the compressor (C) compresses ambient air, driven by a motor that draws electricity from the grid. The compressed gas is transported directly to the Thermal Energy Storage (TES) tank, which is situated in the upper part of the post-mining shaft. The heated compressed air then exchanges heat with the storage material within the heat tank, resulting in a reduction in the temperature of the air to approximately 30

degrees Celsius. The cooled high-pressure air is then directed into the mine shaft space, which serves as the compressed air reservoir. During the charging stage, the pressure in the compressed gas reservoir increases from its minimum value (as designed) to its maximum value (as designed). During the energy storage stage, all machinery is deactivated and the compressed air remains in the mine shaft space. During the discharge stage, the compressed air is directed to the TES tank, where heat is transferred from the storage material to the high-pressure air, and its enthalpy increases before the expansion process. The hot high-pressure air is directed to the expander (EX), which drives a generator (G) that produces electricity. A schematic diagram of the system under consideration is presented in Fig 3.

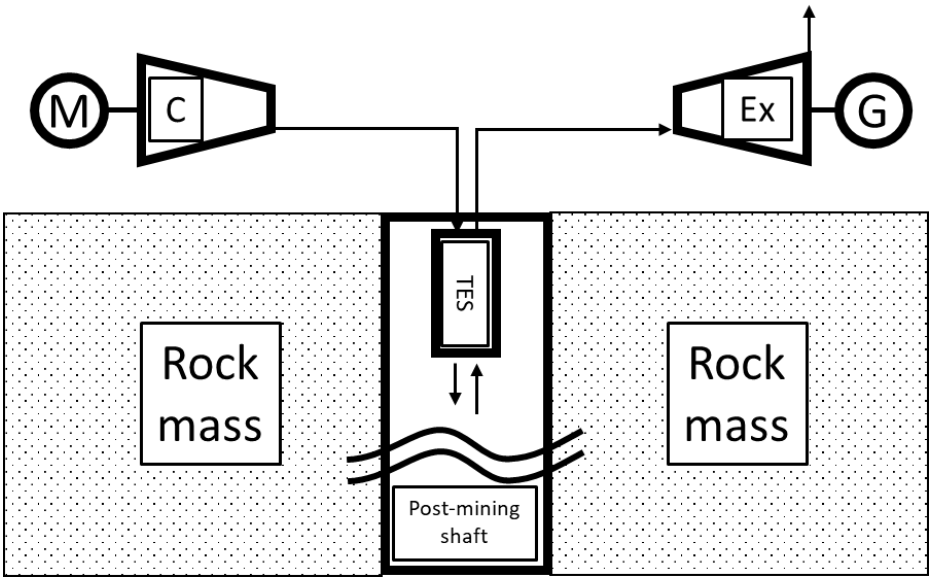

Fig. 3 Diagram of the analyzed adiabatic energy storage system in compressed air (CASE A)

- CASE B

System description: During the charging stage, a two-stage compressor (C1, C2) is employed to compress air in accordance with ambient parameters. The motor that drives the compressor draws electricity from the grid. The compressed gas, following the initial stage of the compressor (C1), is directed to the heat exchanger (HE1), where it exchanges heat with the refrigerant, thereby achieving a certain level of cooling for the compressed air. The compressed air is then directed to the second compressor section (C2). The compressed gas is then directed to the heat exchange tank (TES), which is situated in the upper part of the post-mining shaft. The hot compressed air exchanges heat with the storage material in the heat tank, resulting in a reduction in temperature to approximately 30 degrees Celsius. The cooled high-pressure air is then directed into the mine shaft space, which serves as the compressed air reservoir. During the charging stage, the pressure in the compressed gas reservoir increases from its minimum value (as designed) to its maximum value (as designed). During the energy storage stage, all

machinery is deactivated and the compressed air remains in the mine shaft space. During the discharge stage, the compressed air is directed to the TES tank, where heat is transferred from the storage material to the high-pressure air, and its enthalpy increases prior to the expansion process. The hot high-pressure air is directed to the expander (EX), which drives a generator (G) that produces electricity. A schematic diagram of the system under consideration is presented in Fig 4.

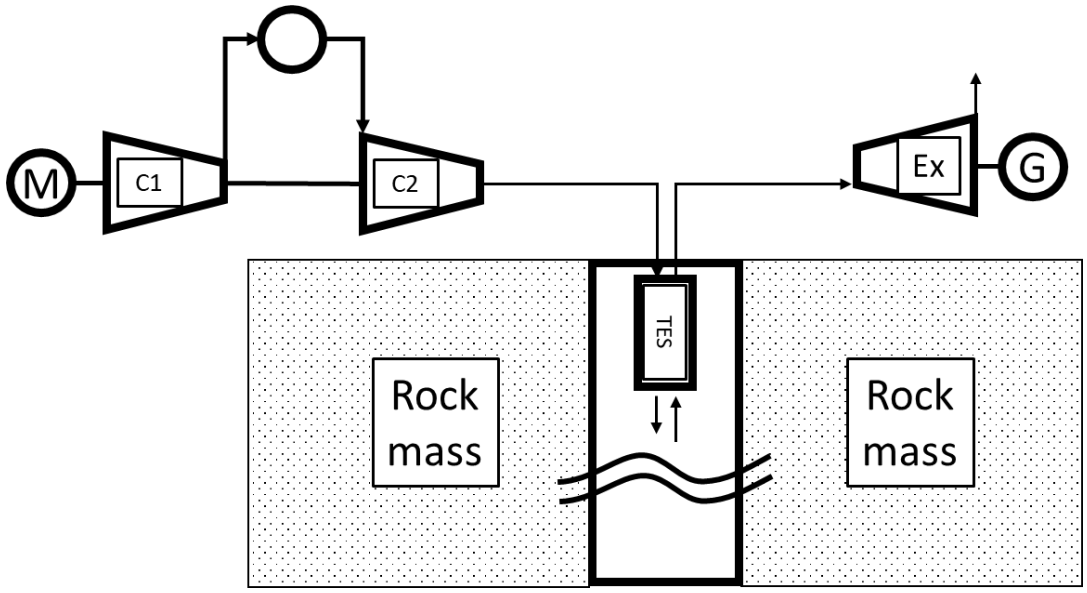

Fig. 4 Diagram of the analyzed adiabatic energy storage system in compressed air (CASE B)

- CASE C

System description: During the charging phase, a three-stage compressor (C1, C2, C3) is employed to compress air at ambient parameters. This compressor is driven by a motor that draws electricity from the grid. The compressed gas, following the initial stage of compression (C1), is directed to the heat exchanger (HE1). At this point, heat is exchanged with the refrigerant, resulting in the cooling of the compressed air to a given temperature. The compressed air is then directed to the second compressor section (C2). Following compression, the air is directed to the second inter-section exchanger (HE2), where it again releases heat to the refrigerant. Subsequently, the cooled air is directed to the third compressor stage (C3), where it is compressed to a specified pressure. The compressed gas is then directed to the heat storage tank (TES), which is located in the upper part of the post-mining shaft. The hot compressed air exchanges heat with the storage material in the heat tank, resulting in the cooling of the air to a temperature of approximately 30°C. The cooled high-pressurised air is then directed into the mine shaft space, which serves as the compressed air reservoir. During the charging stage, the pressure within the compressed gas reservoir increases from its minimum value (as designed) to its maximum value (as designed). During the energy storage stage, all

machinery is kept in standby, with the compressed air remaining within the mine shaft space. During the discharge stage, the compressed air is directed to the TES tank, where heat is transferred from the storage material to the high-pressure air, causing an increase in its enthalpy prior to the expansion process. The hot high-pressure air is directed to the expander (EX), which drives a generator (G) that produces electricity. A schematic diagram of the system under consideration is presented in Fig 5.

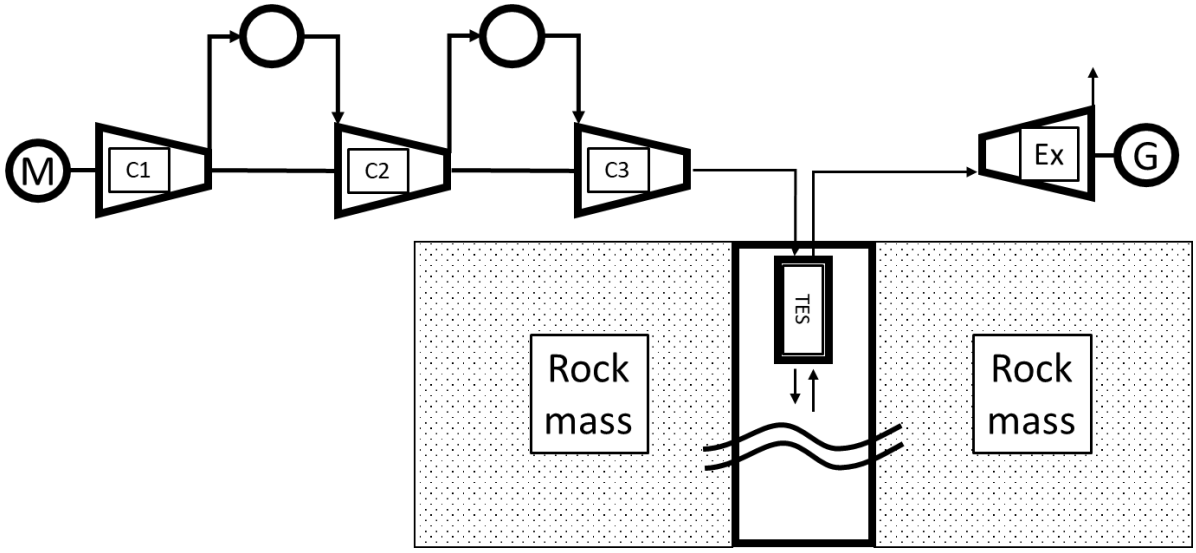

Fig. 5 Diagram of the analyzed adiabatic energy storage system in compressed air (CASE C)

3.3. CCES configuration

System description: The carbon dioxide in this system circulates in a closed loop. There is a Low Pressure Carbon Dioxide (LPT) reservoir in the mine shaft from which a specified flow is drawn for compression by a compressor (C) during the system loading phase. Once compressed, the CO2 transfers heat to thermal oil in a heat exchanger, which is stored in the Thermal Energy Storage (TES). The low temperature compressed CO2 is transferred to the High Pressure Tank (HPT). During the discharge stage of the system, the CO2 from the HPT is routed to the heat exchanger where it is heated using the heat stored in the TES. The high pressure, high temperature carbon dioxide is fed to the expander (Ex) which drives the generator. Behind the expander is a heat exchanger (HE) that enables thermal integration of the CCES system with the energy router and provides low temperature storage of CO2. The carbon dioxide is then routed to a low pressure tank. A schematic diagram of the system under consideration is presented in Fig 6.

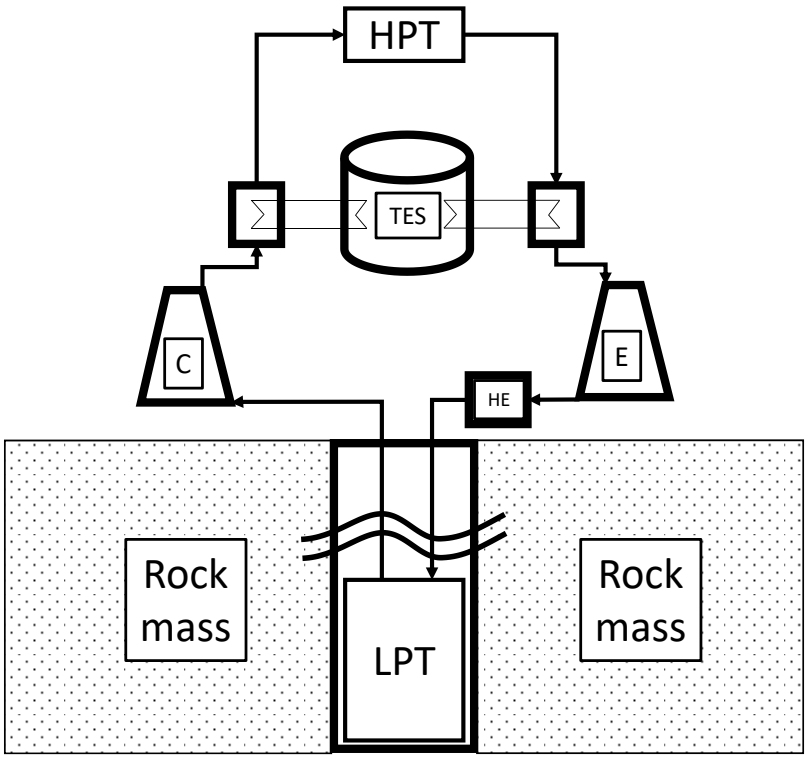

Fig. 6 Diagram of the analyzed adiabatic energy storage system in compressed carbon dioxide

3.4. Assumptions

Table 1 presents the basic assumptions from the configuration of an adiabatic energy storage system in compressed air.

Table 1. Assumptions for modelling an adiabatic energy storage system in compressed air

Item	Value	Unit
Charging stage duration	8	h
Discharging stage duration	4	h
Minimum air pressure in mine shaft	3.6	MPa
Maximum air pressure in mine shaft	5.0	MPa
Ambient pressure	0.1	MPa
Ambient temperature	293.15	K
Nominal length of mine shaft	1000	m
Nominal diameter of mine shaft	9	m
Compressor isentropic efficiency	80	%
Expander isentropic efficiency	80	%
Electromechanical efficiency of expander	98	%

Pressure drop on heat exchangers	2	%
Air temperature after heat exchangers	303.15	K

In accordance with the information presented in the Methodology section, the characteristic curves of the compressor and expander have been adopted and the efficiencies given in Table 1 are those obtained during operation at nominal conditions. Table 2 shows the basic assumptions for the thermal energy storage configuration. The material data for the storage material was taken from the publication [...] based on the results of the project 'Hybrid energy storage system using post-mining infrastructure' in Deliverable 5.1.

Table 2. Assumptions for TES tank (A-CAES)

Item	Value	Unit
TES tank diameter	5	m
TES tank thermal insulation	1	m
Heat accumulator	basalt	-
Specific heat capacity of basalt	920	J/kgK
Density of basalt	2768	kg/m^3
Packed bed porosity	0.38	-
Diameter of basalt particles	16	mm
TES tank volume allowance	20	%

Table 3. Assumptions for modelling an energy storage system in compressed dioxide

Item	Value	Unit
Charging stage duration	8	h
Discharging stage duration	4	h
TES tank energy efficiency	95	%
Pressure drop on heat exchangers	2	%
CO_2 after heat exchangers	303.15	K
Heat accumulator	Therminol VP-1	-
Electromechanical efficiency of expander	98	%

Co-funded by the European Union
Research Fund for Coal & Steel

4. Results analysis

4.1. Comparative analysis of the basic configurations of A-CAES

This section presents the results of the basic thermodynamic analysis of an adiabatic compressed air energy storage system for the three configurations presented in the Methodology section.

- CASE A

Figures 7-9 show the air compressor power, total electricity consumption and air pressure drop values during the charging phase of an A-CAES system with a single-stage compressor.

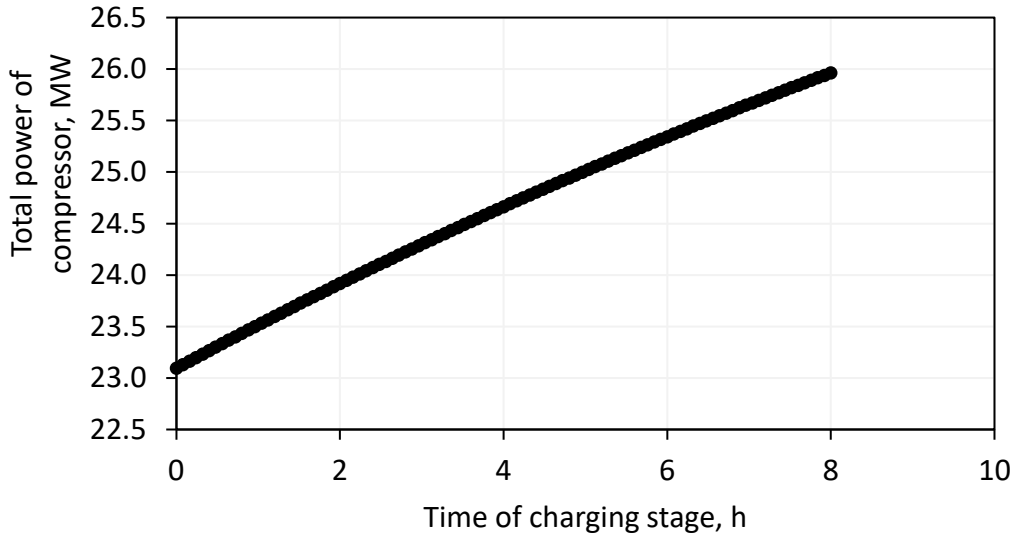

Fig. 7 Power of air compressor during charging stage (Case A)

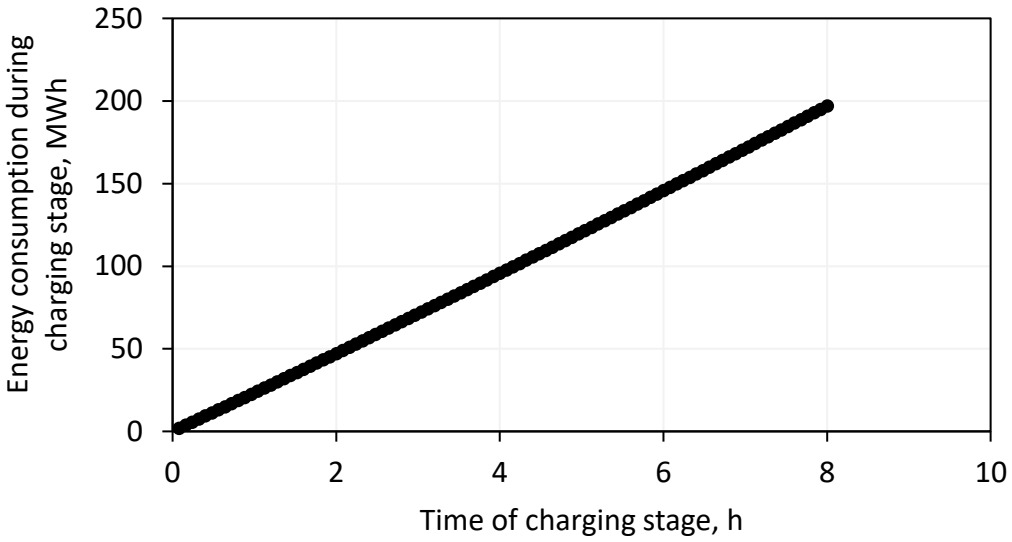

Fig. 8 Energy consumption by air compressor during charging stage (Case A)

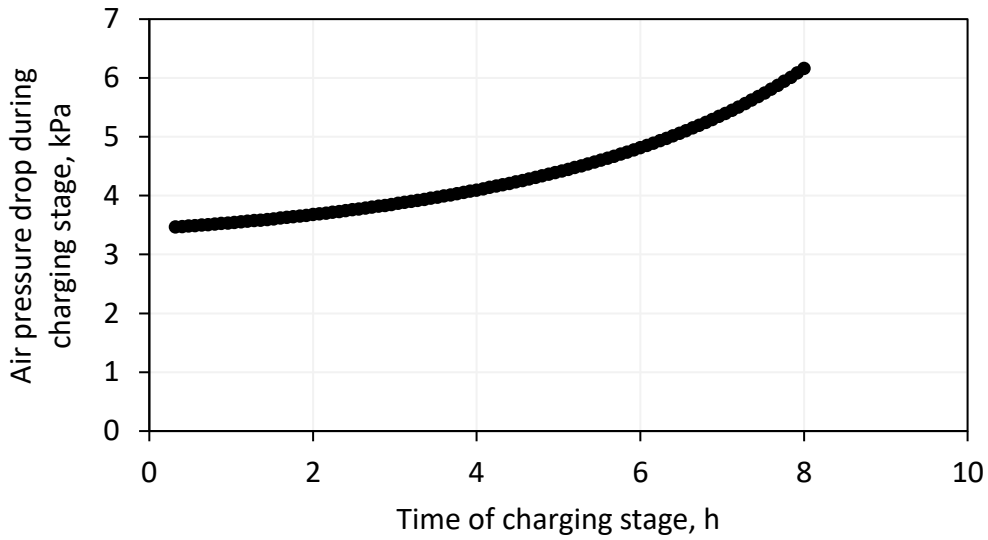

Fig. 9 Air pressure drop on Thermal Energy Storage tank during charging stage (Case A)

Figures 10-12 present data from the air expander power, total power production and air pressure drop values during the discharge stage of the A-CAES system with a single-stage compressor, respectively.

Co-funded by the European Union
Research Fund for Coal & Steel

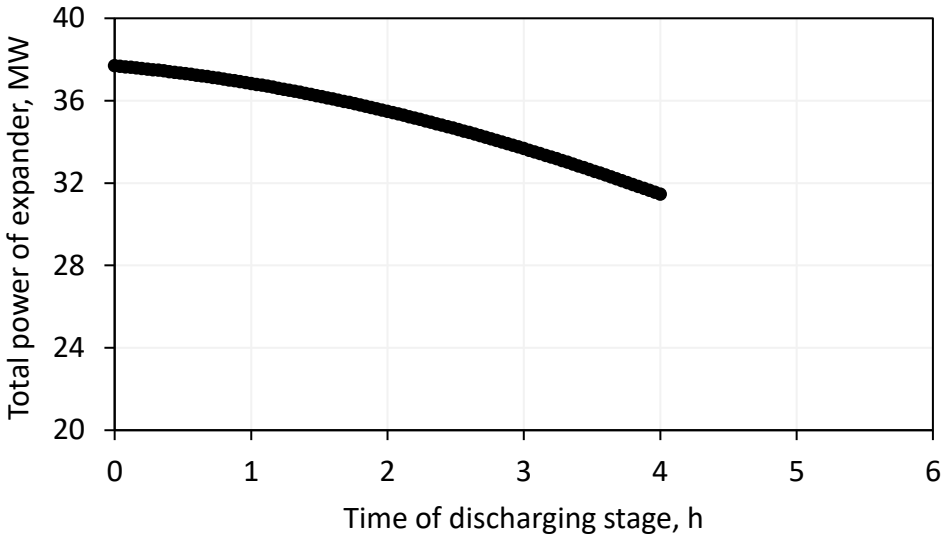

Fig. 10 Power of air expander during discharging stage (Case A)

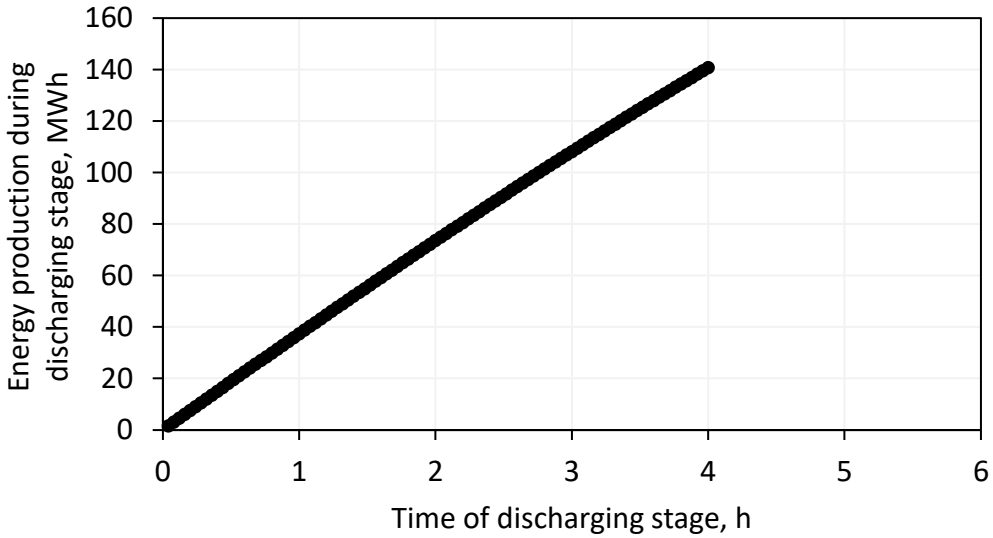

Fig. 11 Energy generation by generator coupled with air expander during discharging stage (Case A)

Co-funded by the European Union
Research Fund for Coal & Steel

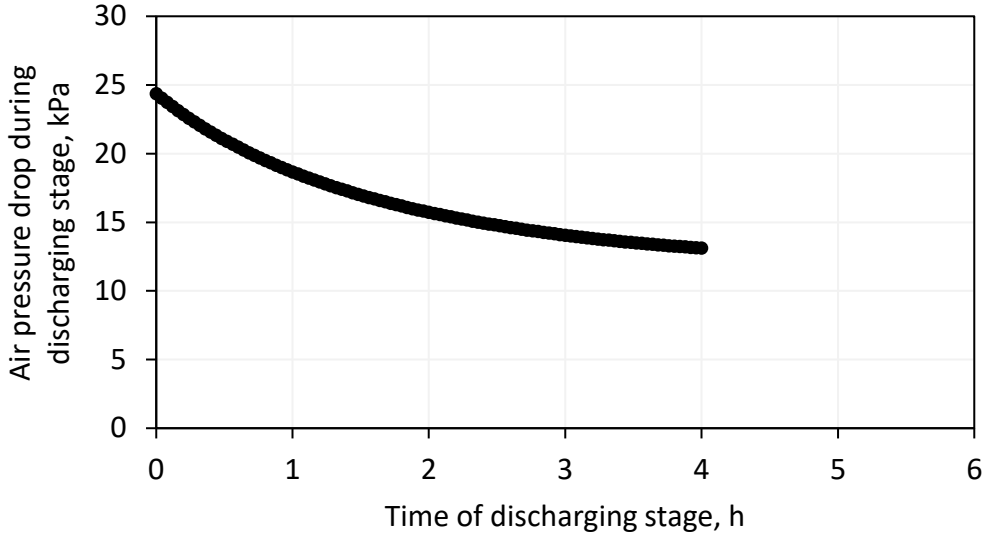

Fig. 12 Air pressure drop on Thermal Energy Storage tank during discharging stage (Case A)

A characteristic feature of a single stage compressor system is the inability to control the maximum temperature of the air after compression. For the assumptions shown in Table 1 and Table 2, the maximum air temperature recorded during the charging stage was 993 K, which directly translates into the need for construction materials with increased temperature resistance. The thermodynamic analysis showed that the efficiency of the adiabatic energy storage system in compressed air with a single stage compressor was 71.45%. The nominal mass flow of compressed air during the charging stage of the system was 35.11 kg/s and the mass flow of expanded air during the discharging stage of the system was 70.22 kg/s.

- CASE B

Figures 13-15 present data from the total power of the air compressor stages, the total electricity consumption and the value of the air pressure drop during the charging stage of an A-CAES system with a two-stage compressor, respectively.

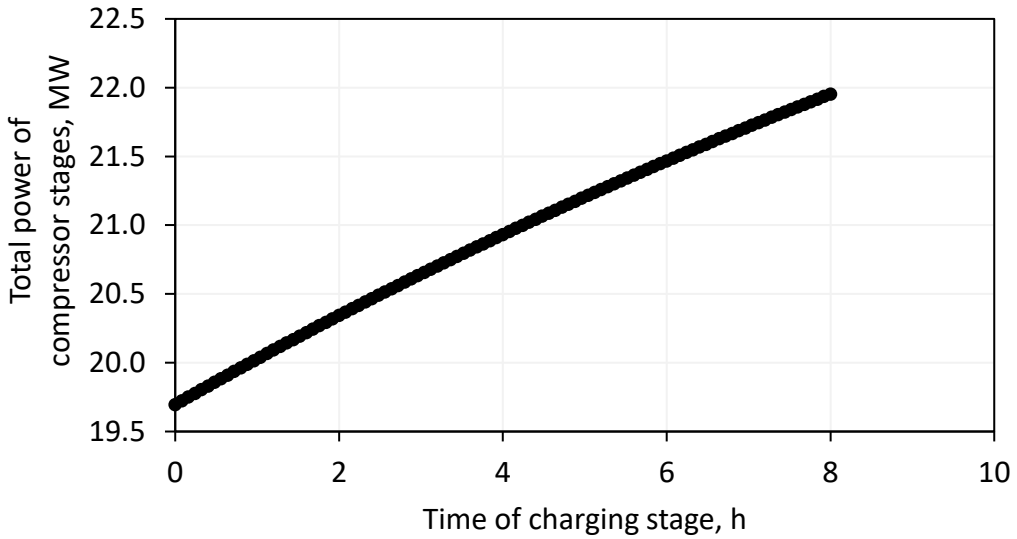

Fig. 13 Total power of two compressor stages during the charging stage of the energy storage system (Case B)

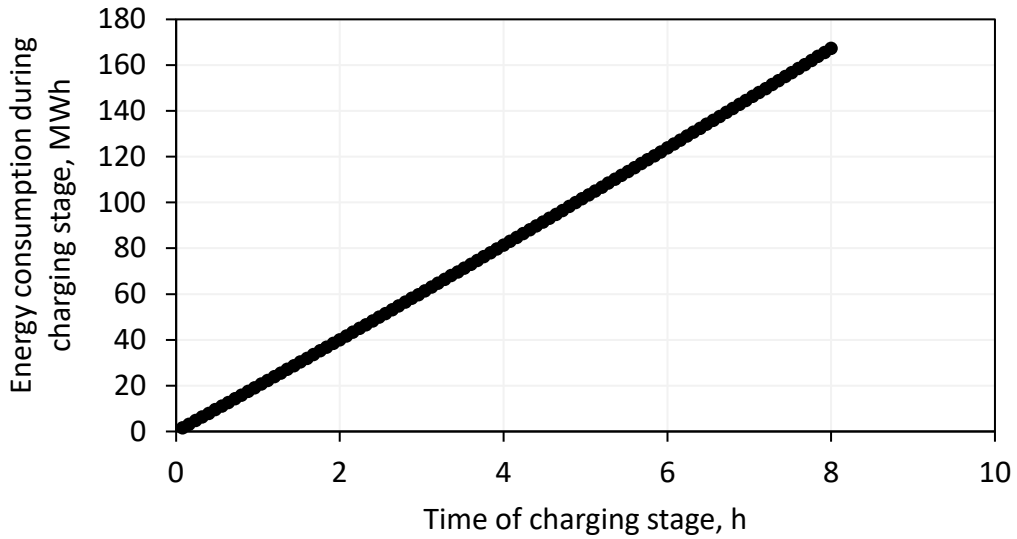

Fig. 14 Energy consumption of two compressor stages during the charging stage of an energy storage system (Case B)

Co-funded by the European Union
Research Fund for Coal & Steel

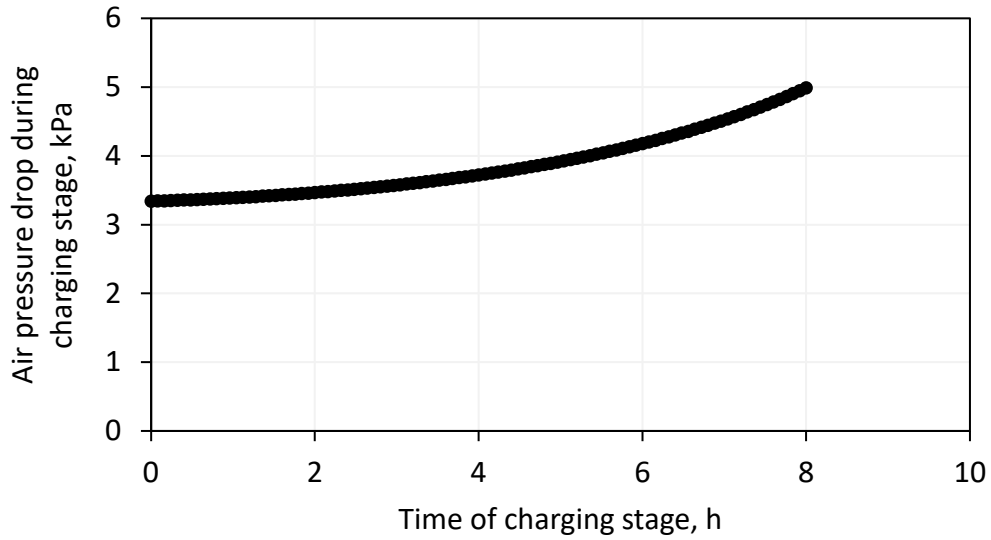

Fig. 15 Air pressure drop on Thermal Energy Storage tank during charging stage (Case B)

Figures 16-18 present data from the air expander power, total power production and air pressure drop values, respectively, during the discharge stage of an A-CAES system with a two-stage compressor.

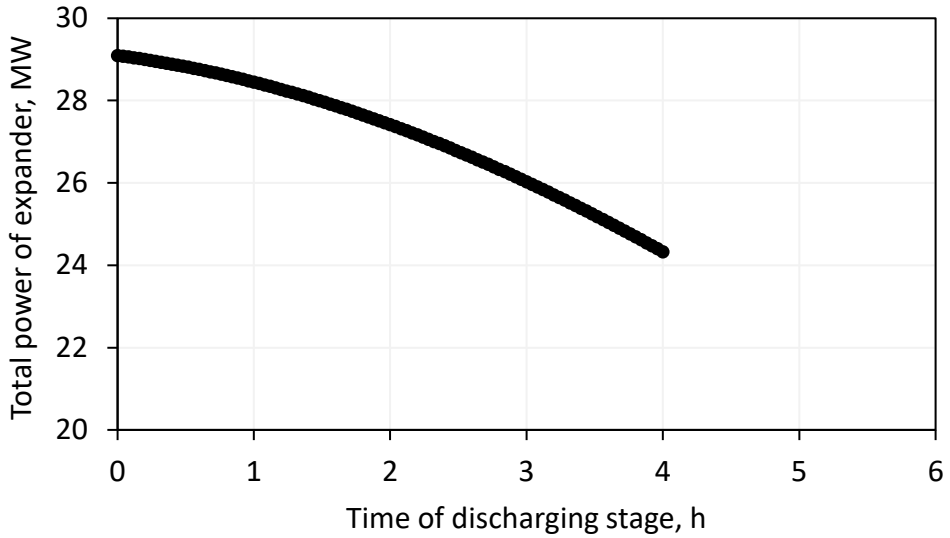

Fig. 16 Expander power during the charging stage of the energy storage system (Case B)

Co-funded by the European Union
Research Fund for Coal & Steel

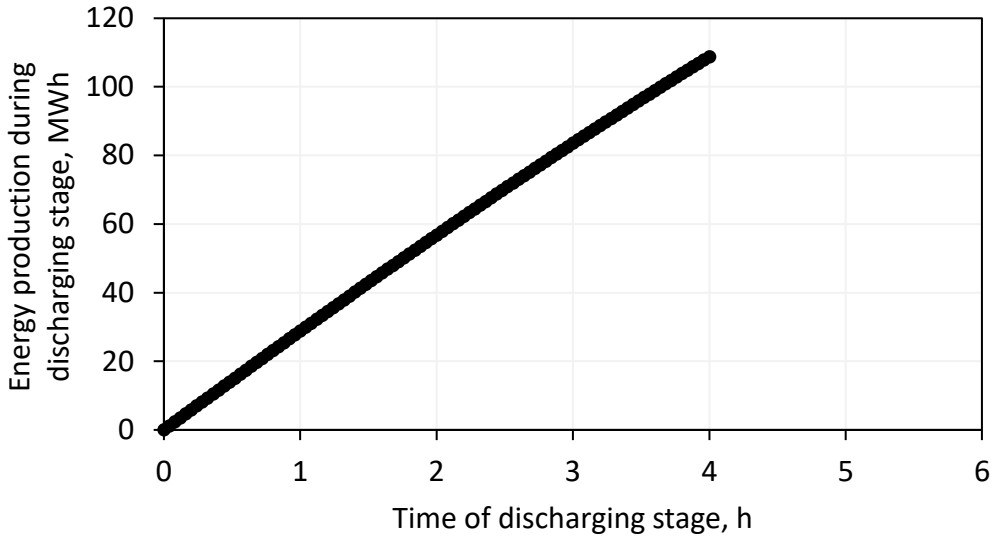

Fig. 17 Energy generation by generator coupled with air expander during discharging stage (Case B)

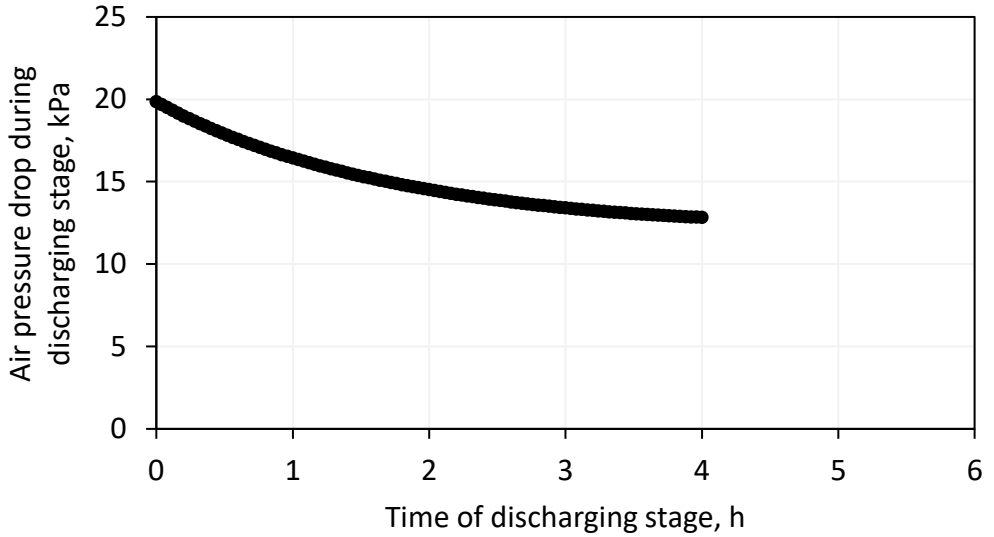

Fig. 18 Air pressure drop on Thermal Energy Storage tank during discharging stage (Case B)

The use of a two-stage air compressor together with interstage cooling enables the desired inlet air temperature to be achieved for thermal energy storage. The results shown in Figures 13-18 were obtained for a maximum inlet temperature of 773.15 K, which corresponds to the limiting parameters defined for the storage material. The reduction in the maximum air temperature also results in a reduction in the value of the air pressure drop due to the reduction in the flow velocity in the TES according to equation Y. The inter-section heat exchanger allows 36 MWh of heat to be extracted at a maximum air temperature of 428 K at the inlet to this heat exchanger. The energy efficiency of the A-CAES system in Variant B is 65%.

- CASE C

Figures 19-21 present data from the total power of the air compressor stages, the total electricity consumption and the value of the air pressure drop during the charging stage of an A-CAES system with a three-stage compressor, respectively.

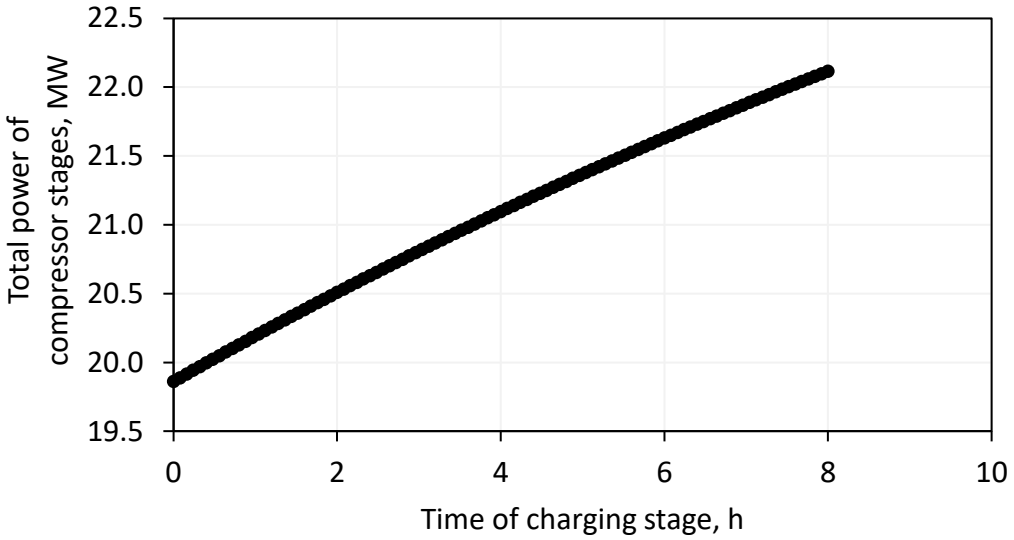

Fig. 19 Total power of three compressor stages during the charging stage of the energy storage system (Case C)

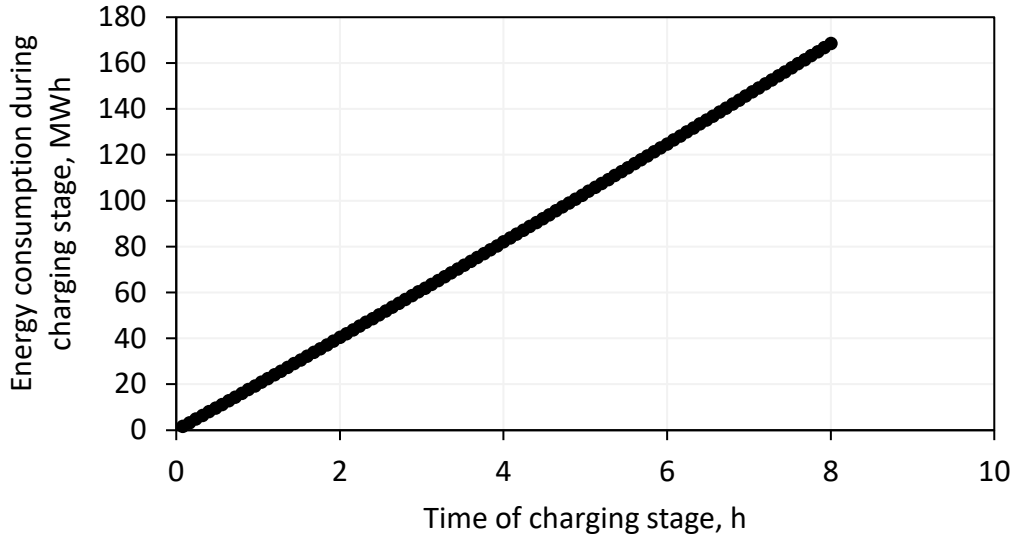

Fig. 20 Energy consumption of three compressor stages during the charging stage of an energy storage system (Case C)

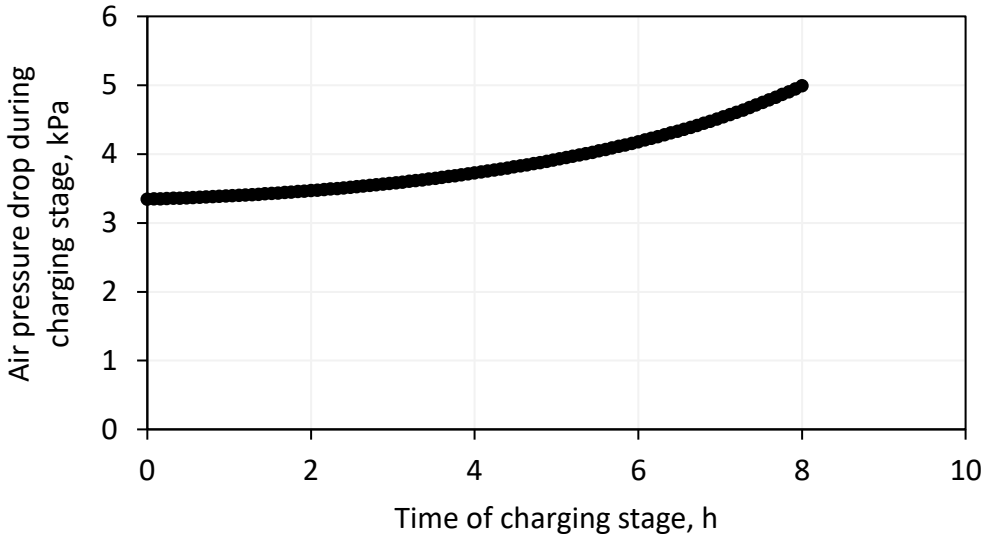

Fig. 21 Air pressure drop on Thermal Energy Storage tank during charging stage (Case C)

Figures 22-24 present data from the air expander power, total power production and air pressure drop values, respectively, during the discharge stage of an A-CAES system with a three-stage compressor.

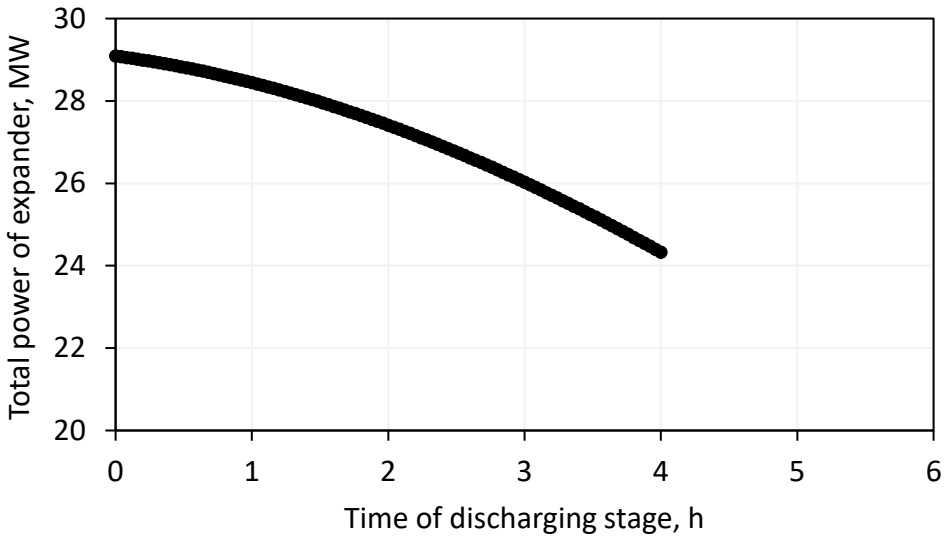

Fig. 22 Expander power during the charging stage of the energy storage system (Case C)

Co-funded by the European Union
Research Fund for Coal & Steel

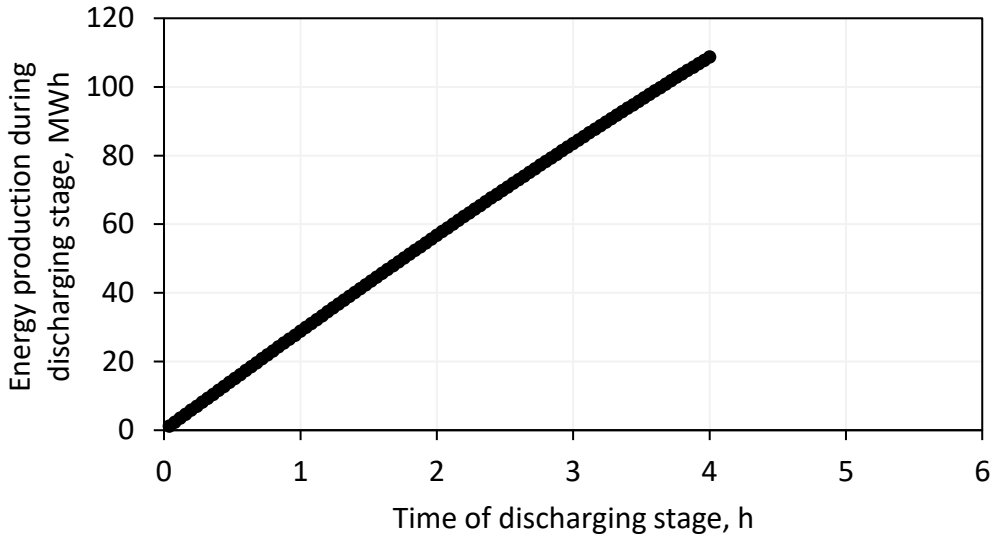

Fig. 23 Energy generation by generator coupled with air expander during discharging stage (Case C)

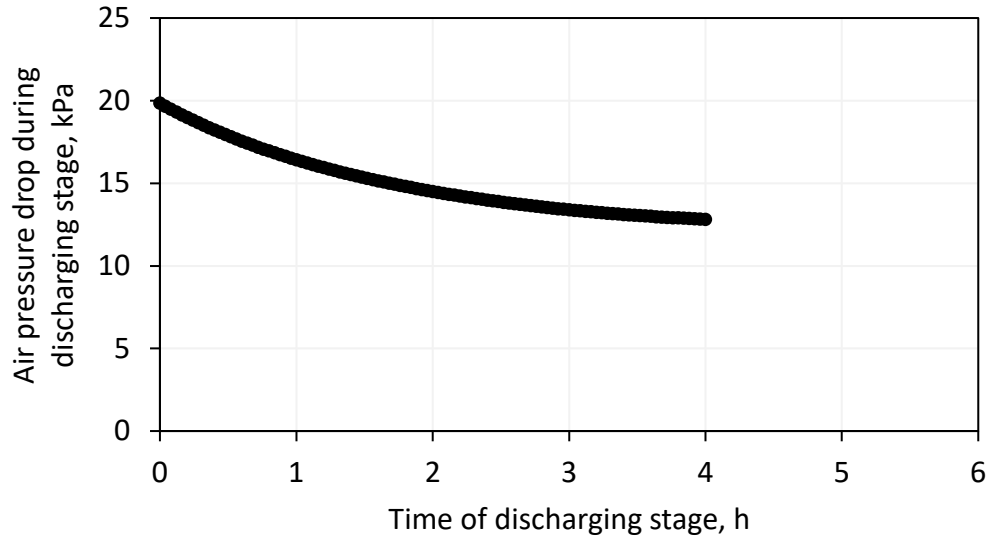

Fig. 24 Air pressure drop on Thermal Energy Storage tank during discharging stage (Case C)

The use of two heat exchangers increases the potential for thermal integration of the compressed air energy storage system with the energy router. By adjusting the compression ratios of the individual compressor stages, it is possible to match the air temperatures achieved upstream of the heat exchangers and the TES. For comparison, the data shown in Figures 19-24 were obtained assuming an inlet air temperature to the TES of 773.15 K - as assumed for Case B. This configuration of the A-CAES system allows 16.9 MWh of heat to be extracted from HE1 and 20.5 MWh of heat to be extracted from HE2. The maximum inlet air temperature to HE1 and HE2 is 362 K and 374 K respectively. The energy efficiency of this configuration is 64.5%.

4.2. A-CAES multi-variant analysis

The analytical model has been employed to conduct a fundamental multivariate analysis, thereby enabling the identification of the influence exerted by specific quantities on the parameters of the energy storage system. Figure 25 illustrates the electricity generated during the discharge phase of the system as a function of the depth of the mine shaft utilized. In this instance, the diameter of the shaft was maintained at a constant value of 9 metres.

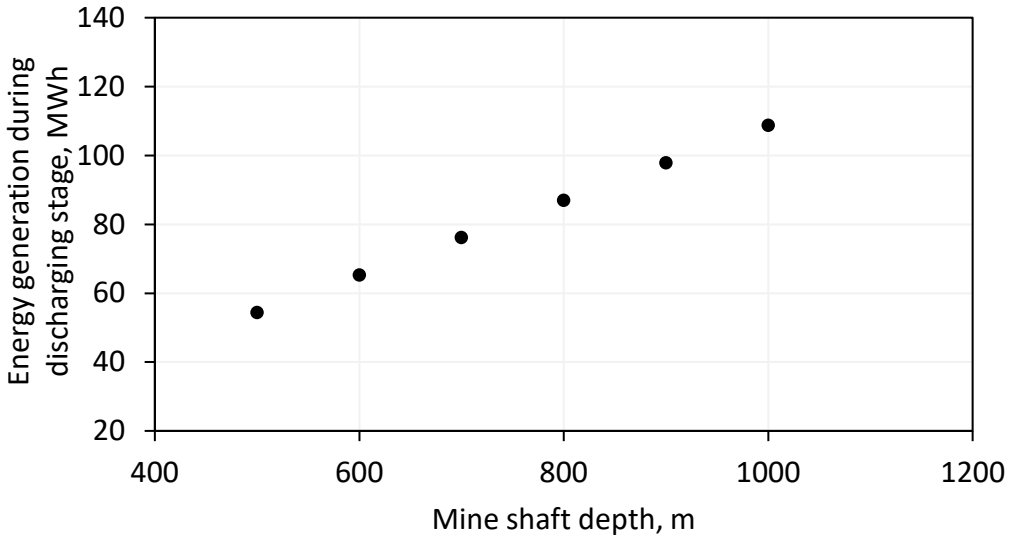

Fig. 25 Dependence of generated electricity on mine shaft depth.

As it has been demonstrated, an increase in shaft depth correlates almost linearly with an increase in generated electricity, which is attributed to an expansion in the volume of the compressed air reservoir. It is, however, important to note that this phenomenon is accompanied by a simultaneous increase in electricity consumption by the compressors. Figure 26 illustrates the heat extracted from the inter-section heat exchanger for case B with a two-section air compressor. Figure 27 illustrates the maximum allowable inlet air temperature to the heat exchanger. These values are contingent upon the desired inlet air temperature to the thermal energy storage system.

Co-funded by the European Union
Research Fund for Coal & Steel

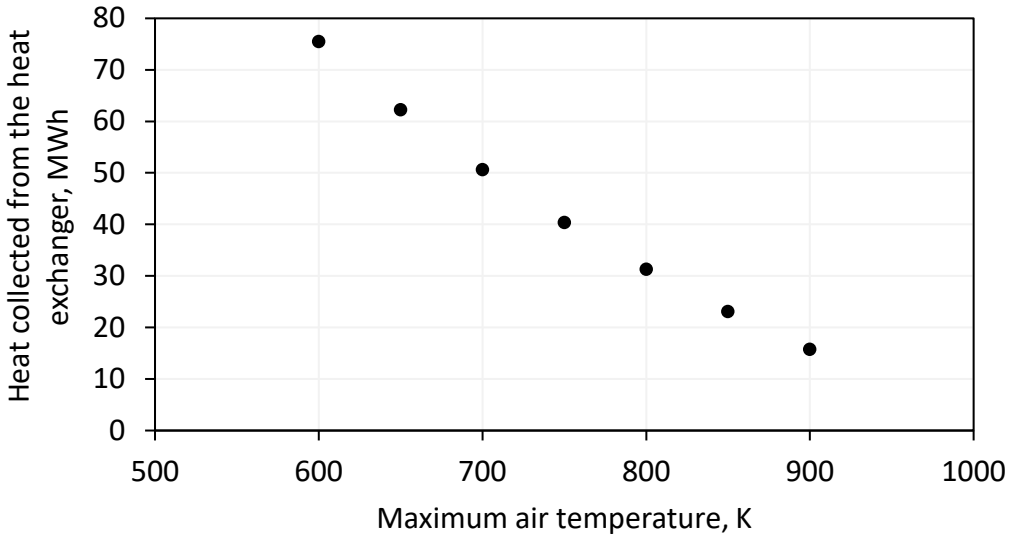

Fig. 26 Heat recovered in an inter-section heat exchanger in an energy storage system with a two-stage air compressor (Case B)

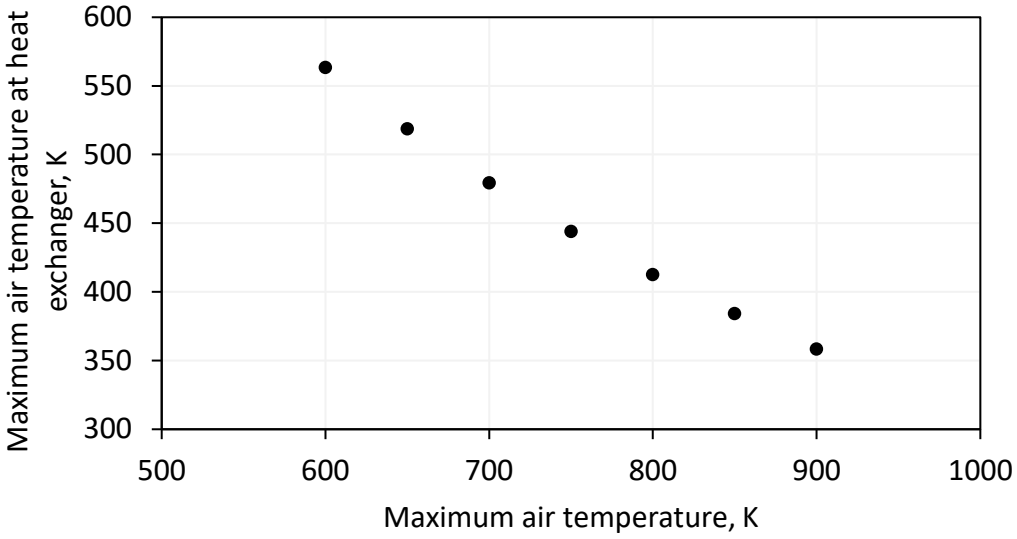

Fig. 27 Maximum air temperature in an inter-sectional heat exchanger in an energy storage system with a two-stage air compressor (Case B)

Figure 28 illustrates the correlation between the heat transferred in HE1 and HE2 and the anticipated inlet air temperature to the TES in a system equipped with a three-stage air compressor during the charging phase of the system. Additionally, Figure 29 depicts the relationship between the maximum air temperature in the heat exchangers and the expected inlet air temperature to the TES.

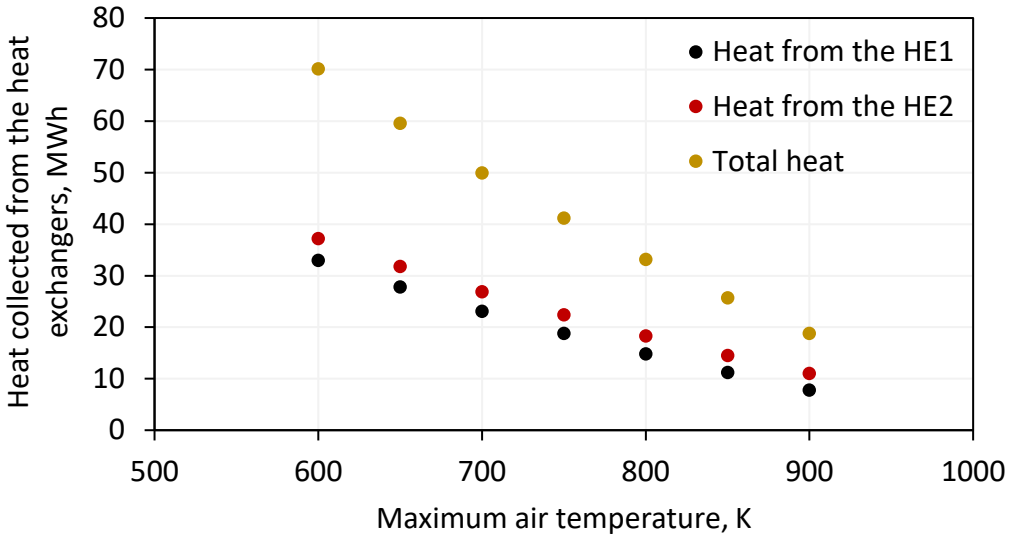

Fig. 28 Heat transferred in inter-section heat exchangers in an energy storage system with a three-stage air compressor (Case C)

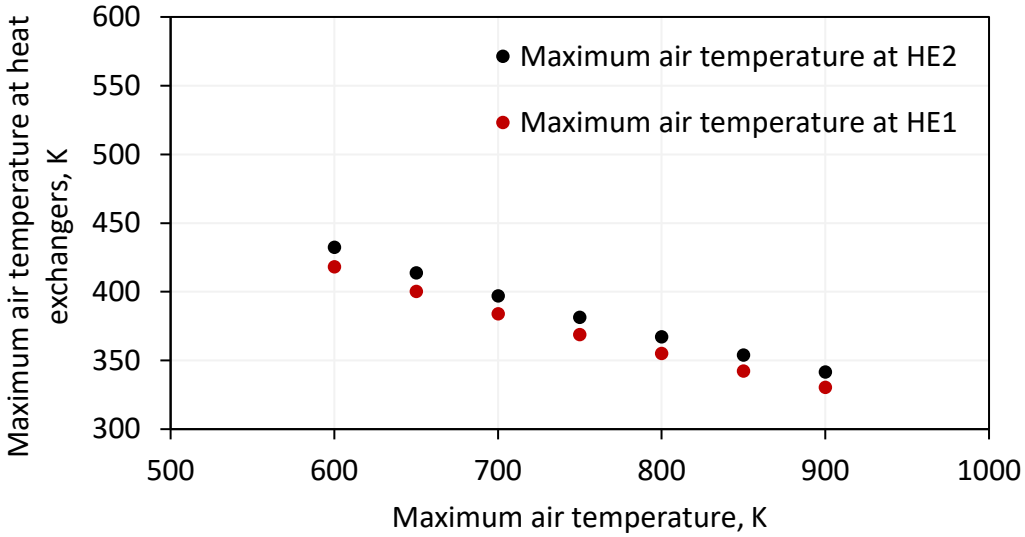

Fig. 29 Maximum air temperature in inter-sectional heat exchangers in an energy storage system with three-stage air compressor (Case C)

In all cases analysed, a reduction in the expected inlet air temperature to the TES has been observed to result in an increase in both the air temperature on the heat exchangers and the heat transferred to the coolant. This is a direct consequence of the alteration in compression ratio and the corresponding change in power output between the first and last compression stages.

Co-funded by the European Union
Research Fund for Coal & Steel

4.3. CCES thermodynamic analysis

Figure 30 shows the dependence of the volume of the high-pressure vessels on the CO2 pressure in the low-pressure tank. Figure 31 shows the dependence of the electricity consumption of the carbon dioxide compressor on the CO2 pressure in the low pressure vessel. Figure 32 presents the dependence of electricity generation on the pressure of carbon dioxide in the low-pressure vessel. Figure 33 presents the dependence of the energy efficiency of the compressed carbon dioxide energy storage system on the pressure in the LPT tank.

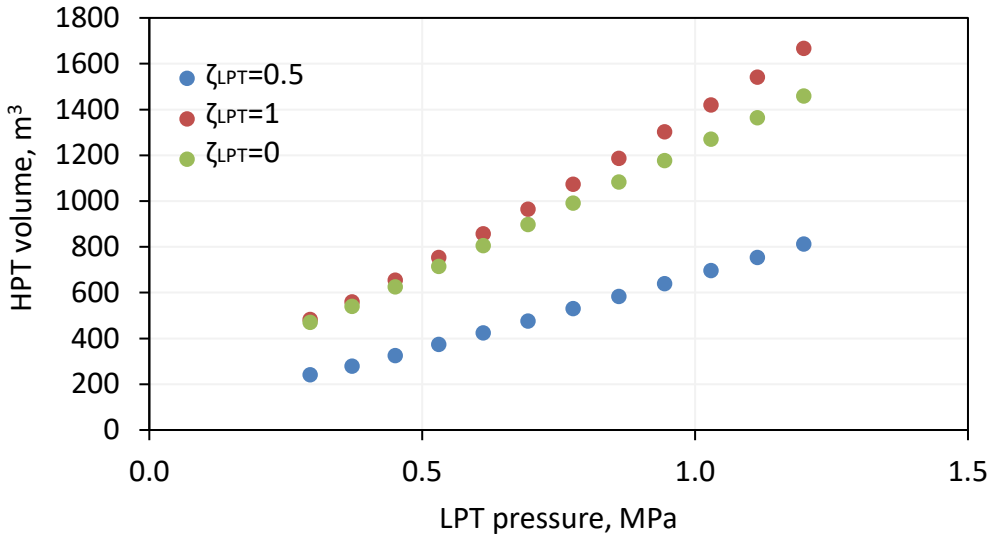

Fig. 30 Dependence of the volume of high-pressure tanks on the pressure in the LPT

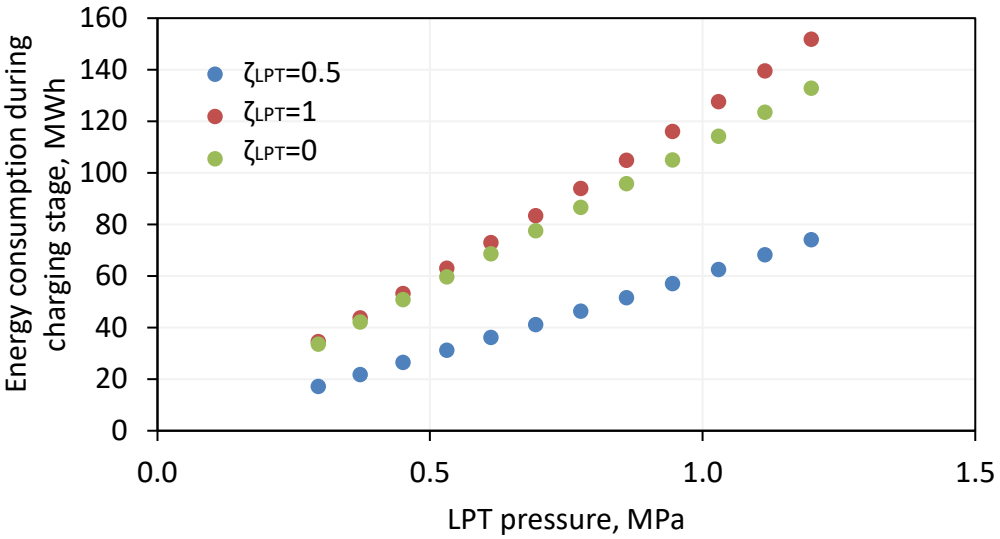

Fig. 31 Dependence of electricity consumption on the pressure in the LPT

Co-funded by the European Union
Research Fund for Coal & Steel

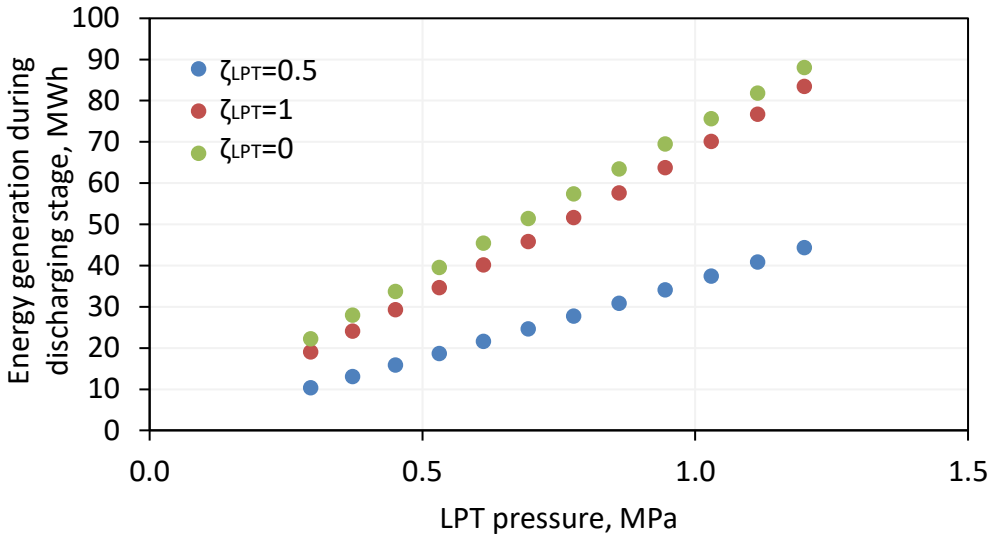

Fig. 32 Dependence of electricity production on LPT pressure

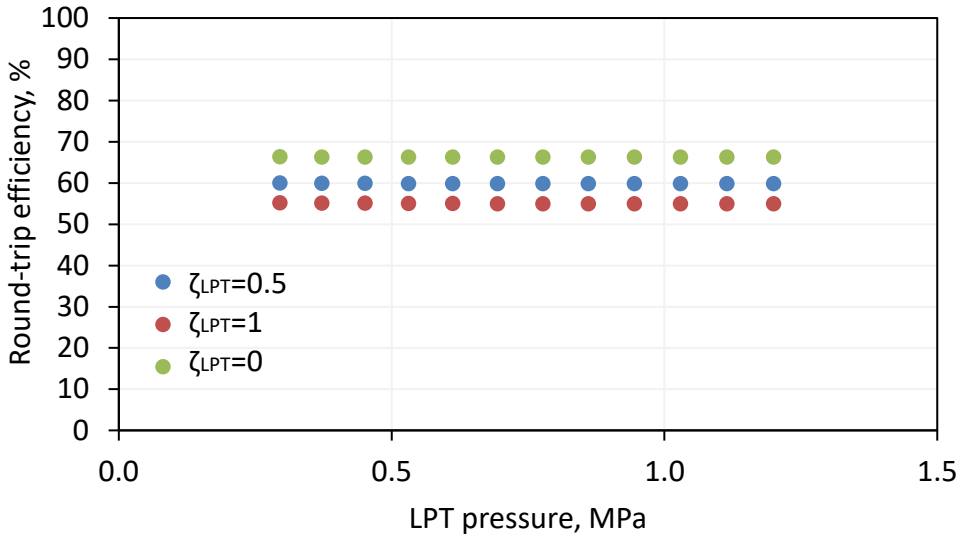

Fig. 33 Dependence of energy storage system efficiency on LPT tank pressure

The characteristics of the TES tank employed in the modelling of the compressed carbon dioxide energy storage system permit a constant CO_2 temperature during the discharge stage of the system. The highest energy efficiency of the compressed carbon dioxide energy storage system is achieved in the case of an isobaric LPT tank ($\xi_{LPT} = 0$). As the pressure in the LPT increases, an increase in electricity consumption and production is observed, which is directly related to the increase in the amount of CO_2 in the system.

Co-funded by the European Union
Research Fund for Coal & Steel

4.4. CCES multi-variant analysis

Figures 35-37 show the results of the multivariate analysis. Figure 35 presents the temperature dependence of CO_2 on the heat exchanger as a function of pressure in the LPT and the value of the ξ_{LPT} coefficient.

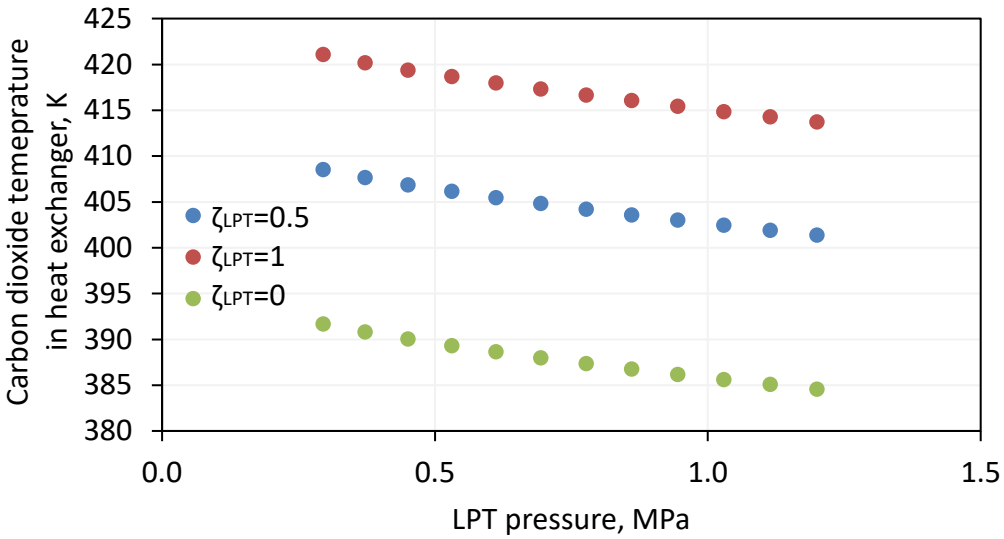

Fig. 35 Temperature dependence of CO2 in the heat exchanger on pressure in the LPT tank

As evidenced by the presented data, the CO2 temperature is consistently above 385 K for all variants under investigation. Consequently, it is feasible to generate heat with an average temperature potential through thermal integration with the energy router. Figure 36 illustrates the energy efficiency of the system when the maximum heat storage temperature in the TES is 300 °C and the isentropic efficiency of the compressor and expander is 80%.

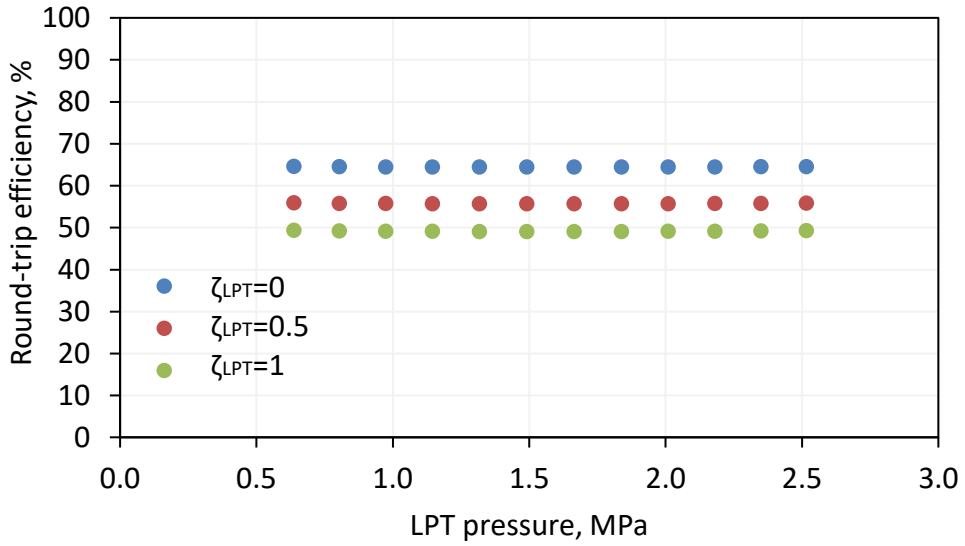

Co-funded by the European Union
Research Fund for Coal & Steel

Fig. 36 Dependence of energy storage system efficiency on LPT tank pressure (Case 300 ºC, $\eta_{iC} = \eta_{iEx}$ =80%)

`Figure 37 presents the energy efficiency values of the compressed carbon dioxide energy storage system for the case where the maximum heat storage temperature in the TES is 300 ºC and the isentropic efficiency of the compressor and expander is 90%.

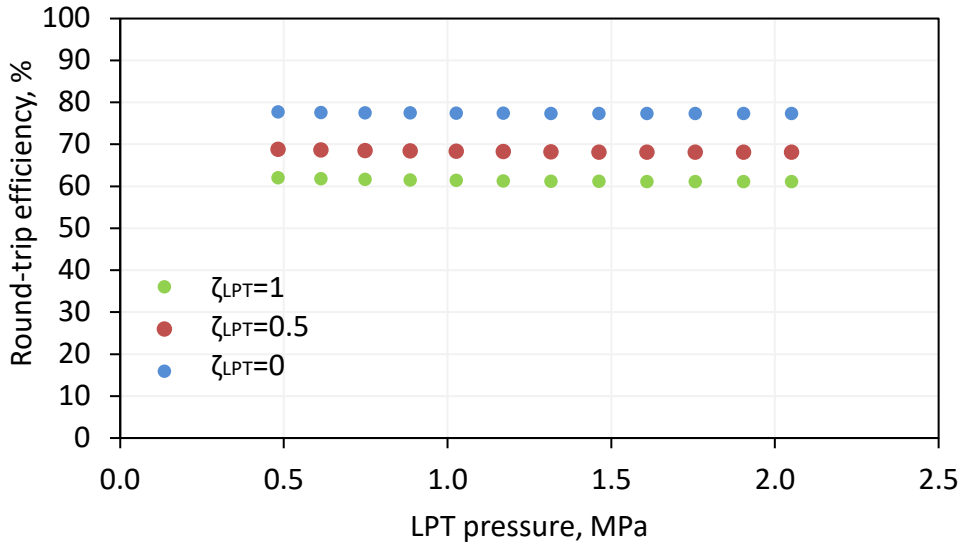

Fig. 37 Dependence of energy storage system efficiency on LPT tank pressure (Case 300 ºC, $\eta_{iC} = \eta_{iEx}$ =90%)

5. Summary and conclusion

Based on the analyses carried out, it has been found:

- The adiabatic compressed air energy storage system with a single-stage compressor exhibits the highest energy efficiency of the configurations tested. This configuration has the highest inlet air temperature to the TES tank. However, the absence of a heat exchanger in the system precludes potential thermal integration with the energy router. Consequently, this configuration is unsuitable for further research into the implementation of an energy storage system using a mine shaft.
- The A-CAES system in configurations B and C exhibits a comparable energy efficiency of approximately 65%. These systems are distinguished by their capacity to modify the compression ratios, or the quantity of heat transferred in the heat exchangers, in accordance with the demands of the other components within the energy router.
- The mine shafts that were subjected to analysis as part of the project can be characterised by a satisfactory compressed air reservoir volume. This volume has been demonstrated to have a direct impact on the total power generation that occurs during the discharge stage.
- Energy storage in compressed carbon dioxide is a far less mature and verified An energy storage system utilising compressed carbon dioxide can achieve energy efficiencies of between 50% and 67%, contingent on the variant under consideration. The incorporation of a heat exchanger between the expander and the LPT facilitates the integration of any variant of the system with an energy router.
- Further analysis in the field of energy storage in compressed carbon dioxide is required, with particular attention paid to variants with a parameter of $\xi_{LPT} = 0$ and $\xi_{LPT} = 1$.

6. Bibliography

1. Rusin, A.; Wojaczek, A. Changes in the Structure of the Polish Energy Mix in the Transition Period to Ensure the Safety and Reliability of Energy Supplies. *Energy* **2023**, *282*, 128831, doi:10.1016/j.energy.2023.128831.
2. Ochmann, J.; Jurczyk, M.; Rusin, K.; Rulik, S.; Bartela, Ł.; Uchman, W. Solution for Post-Mining Sites: Thermo-Economic Analysis of a Large-Scale Integrated Energy Storage System. *Energies* **2024**, *17*, 1970, doi:10.3390/en17081970.
3. Bartela, Ł.; Ochmann, J.; Waniczek, S.; Lutyński, M.; Smolnik, G.; Rulik, S. Evaluation of the Energy Potential of an Adiabatic Compressed Air Energy Storage System Based on a Novel Thermal Energy Storage System in a Post Mining Shaft. *Journal of Energy Storage* **2022**, *54*, 105282, doi:10.1016/j.est.2022.105282.
4. Stanek, B.; Ochmann, J.; Bartela, Ł.; Brzuszkiewicz, M.; Rulik, S.; Waniczek, S. Isobaric Tanks System for Carbon Dioxide Energy Storage – The Performance Analysis. *Journal of Energy Storage* **2022**, *52*, 104826, doi:10.1016/j.est.2022.104826.

5. Bartela, Ł.; Skorek-Osikowska, A.; Dykas, S.; Stanek, B. Thermodynamic and Economic Assessment of Compressed Carbon Dioxide Energy Storage Systems Using a Post-Mining Underground Infrastructure. *Energy Conversion and Management* **2021**, *241*, 114297, doi:10.1016/j.enconman.2021.114297.
6. Chen, H.; Wang, H.; Li, R.; Sun, H.; Zhang, Y.; Ling, L. Thermo-Dynamic and Economic Analysis of a Novel Pumped Hydro-Compressed Air Energy Storage System Combined with Compressed Air Energy Storage System as a Spray System. *Energy* **2023**, *280*, 128134, doi:10.1016/j.energy.2023.128134.
7. CAES Overview, http://www.apexcaes.com/caes.
8. Borzea, C.; Vlăducă, I.; Ionescu, D.; Petrescu, V.; Niculescu, F.; Nechifor, C.; Vătășelu, G.; Hanek, M. Compressed Air Energy Storage Installation for Renewable Energy Generation. *E3S Web Conf.* **2019**, *112*, 02010, doi:10.1051/e3sconf/201911202010.
9. Guo, C.; Xu, Y.; Guo, H.; Zhang, X.; Lin, X.; Wang, L.; Zhang, Y.; Chen, H. Comprehensive Exergy Analysis of the Dynamic Process of Compressed Air Energy Storage System with Low-Temperature Thermal Energy Storage. *Applied Thermal Engineering* **2019**, *147*, 684–693, doi:10.1016/j.applthermaleng.2018.10.115.
10. Ochmann, J.; Rusin, K.; Jurczyk, M.; Rulik, S.; Bartela, Ł. Theory of Time Constant Correlation of a Porous Bed Thermal Energy Storage Tank - Experimental and Numerical Proof of Concept. *Energy* **2024**, *308*, 132956, doi:10.1016/j.energy.2024.132956.
11. Niven, R.K. Physical Insight into the Ergun and Wen & Yu Equations for Fluid Flow in Packed and Fluidised Beds. *Chemical Engineering Science* **2002**, *57*, 527–534, doi:10.1016/S0009-2509(01)00371-2.